Received May 27, 2020, accepted June 15, 2020, date of publication June 19, 2020, date of current version June 30, 2020.

Digital Object Identifier 10.1109/ACCESS.2020.3003597

Noise Reduction of LiDAR Signal via Local Mean Decomposition Combined With Improved Thresholding Method

LUYAO ZHANG[1], JIANHUA CHANG[1,2], HONGXU LI[1], ZHEN XING LIU[1,3], SHUYI ZHANG[1], AND RENGXIANG MAO[1]

[1]Jiangsu Key Laboratory of Meteorological Observation and Information Processing, Nanjing University of Information Science and Technology, Nanjing 210044, China
[2]Collaborative Innovation Center of Atmospheric Environment and Equipment Technology, Nanjing University of Information Science and Technology, Nanjing 210044, China
[3]Department of Information Technology, Taizhou Polytechnic College, Taizhou 225300, China

Corresponding author: Jianhua Chang (jianhuachang@nuist.edu.cn)

This work was supported in part by the National Natural Science Foundation of China under Grant 61875089, in part by the Project Funded by the Priority Academic Program Development of Jiangsu Higher Education Institutions, China, under Grant 1081080015001, and in part by the Postgraduate Research and Practice Innovation Program of Jiangsu Province under Grant SJCX19_0308.

ABSTRACT The echo signal of light detection and ranging (LiDAR) system is easily disturbed by various noises under the influence of intense background light. The signal to noise ratio (SNR) decreases with increasing distance, which seriously affects the retrieval accuracy of the LiDAR system. This paper combines local mean decomposition and an improved thresholding method (LMD-ITM) to process the Lidar signal with a lot of noise, so as to avoid the loss of useful information. In this research, the correlation coefficient and energy entropy are used to distinguish between the relevant and irrelevant components decomposed by the local mean decomposition. Subsequently, the improved thresholding method is applied to process the irrelevant components. It can extract the effective signals which are difficult to be separated from the high-frequency signals. Finally, all components are reconstructed to get the denoising signal. The experimental results demonstrate that this method can effectively avoid the short-range migration, suppress the long-range noise, and adapt to different weather conditions. Compared with the previous denoising method, the proposed method increases the SNR by about 15%.

INDEX TERMS LiDAR signal denoising, local mean decomposition, correlation coefficient, thresholding method.

I. INTRODUCTION

The light detection and ranging (LiDAR) is an active remote sensing technique applied to survey atmospheric parameters [1]. LiDAR can measure temperature, wind speed, atomic and molecular concentrations, aerosol and cloud properties, and a series of parameters to reflect the atmospheric situation [2]. LiDAR data are usually multiplied by the square of the distance because this processing can reduce the influence of the distance on the signal. However, the real signals may be submerged by the noise in this process because the components of noise are amplified accordingly [3]. The noise can vastly reduce the detection precision and available working range because the laser beam emitted low energy. In recent years, many researchers have focused on this problem and tried to break through the critical bottleneck via signal denoising. The main cause of noise pollution comes from dark current noise, signal-induced quantum noise, amplifier noise, and background noise [4]. These noises do not interfere with each other, and the total noise can be obtained by summing the independent random variables. The noise in the LiDAR signal has the characteristics of continuous amplitude and random phase in time, which can be regarded as a typical nonlinear and nonstationary signal [5]. Hence, removing noise is a necessary but difficult task.

In previous studies, the methods of LiDAR signal denoising have been extensively studied, such as the moving average (MA) [6], Kalman filtering (KF) [7], Fourier transform (FT) [8], wavelet transform (WT) [9].

The associate editor coordinating the review of this manuscript and approving it for publication was Pia Addabbo.

The empirical mode decomposition (EMD) method, which was originally proposed by Huang *et al.*, has demonstrated outstanding performance when applied to the nonlinear and nonstationary signals [10]. Nevertheless, EMD still has a few disadvantages, such as the end effects and the mode mixing. The complete ensemble empirical mode decomposition with adaptive noise (CEEMDAN) was proved to be an improvement on EMD, which increases the reconstruction accuracy [11]. The variational mode decomposition (VMD) technique can achieve a nice smoothing effect using its Wiener filtering characteristics. The research results show that the VMD combined with whale optimization algorithm (VMD-WOA) can also achieve better results in LiDAR signal denoising [12]. The common point of the above methods is that the LiDAR signal is decomposed into a series of components and removed the high-frequency components containing noise to realize the denoising. However, simply filtering out the high-frequency components will lead to the loss of useful information contained in the high-frequency components, which is not conducive to the accurate inversion of the signal.

Jonathan S. Smith successfully used the local mean decomposition (LMD) method to handle the electroencephalogram signal [13]. It can be applied in many fields as an adaptive signal decomposition method. The multicomponent signal can be adaptively decomposed into a train of product functions (PFs) with physical significance by this method [14], [15]. LMD can achieve the frequency directly and instantaneous envelope amplitude without the Hilbert Transform [16], so it would not be affected by the limitation of the Hilbert Transform [17]. Because of the superiority of LMD, it is very suitable for the time-frequency analysis of the nonstationary signals. By comparing with EMD, it can be seen that LMD can overcome the limitation of the end effect and reduce the influence of the mode mixing problems in EMD [18], [19].

In the paper, we put forward a technique for denoising the LiDAR signal, which integrates LMD and improved thresholding method (LMD-ITM). The proposed method uses LMD to decompose the LiDAR signal into a group of components, and the energy entropy and the correlation coefficient are used to determine whether the components are related. Subsequently, the improved thresholding method is used to the irrelevant components to extract useful information, and all the components are reconstructed to achieve noise filtering. Experiments with the simulated signal and real LiDAR signal are evaluated to prove the superiority of LMD-ITM approach.

II. BASIC THEORY OF LMD METHOD

LMD method is a double cycle process. It is utilized to extract a group of the best product functions from the original discrete signal by the outer cycle and obtained the frequency modulation signal and the reserved signal through the inner cycle [20].

LMD decomposes a complex signal into a set of product functions through two iterations, every product function obtained by LMD is the product of envelope signal and pure frequency modulation signal. The specific operation of LMD decomposition can be divided into the following seven steps:

Step 1. Find the maxima and minima as the local extremes in the original signal $x(t)$. The mean value m_i can be calculated by two consecutive extrema n_i and n_{i+1}.

$$m_i = \frac{n_i + n_{i+1}}{2}. \tag{1}$$

All the mean values m_i of two successive extremes are connected by straight lines, and then the local mean function $m_{11}(t)$ can be formed using the smoothing algorithm to smooth the local means m_i.

Step 2. Corresponding envelope estimate a_i can be obtained by

$$a_i = \frac{|n_i - n_{i+1}|}{2}. \tag{2}$$

Using the smoothing algorithm to deal with the envelope estimate a_i, we can get the corresponding local mean function $m_{11}(t)$ and local magnitude function $a_{11}(t)$. In this experiment, the moving average (MA) is used as the smoothing algorithm, in which the cut-off frequency is determined by the fixed subset size. Fig. 1 shows a raw signal with its corresponding the local mean and the local magnitude functions. The local mean and the local magnitude become smoother after applying the MA.

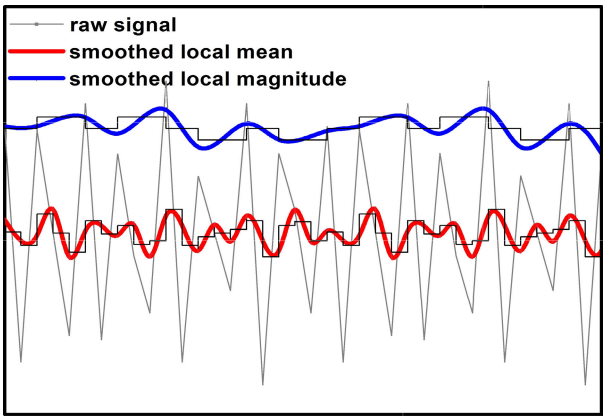

FIGURE 1. Five signals (raw signal, local mean, smoothed local mean, local magnitude, and smoothed local magnitude) defined in LMD.

Step 3. On the basis of $x(t)$, $m(t)$ to calculate the estimated zero-mean signal $h_{11}(t)$. The local mean function $m_{11}(t)$ is subtracted from the original signal $x(t)$, and the estimated zero-mean signal $h_{11}(t)$ is given by

$$h_{11}(t) = x(t) - m_{11}(t). \tag{3}$$

Step 4. The estimated frequency modulation signal $s_{11}(t)$ can be calculated according to the following formula:

$$s_{11}(t) = \frac{h_{11}(t)}{a_{11}(t)}. \tag{4}$$

Using the same method, the envelope function $a_{12}(t)$ of $s_{11}(t)$ can be calculated. The envelope function should

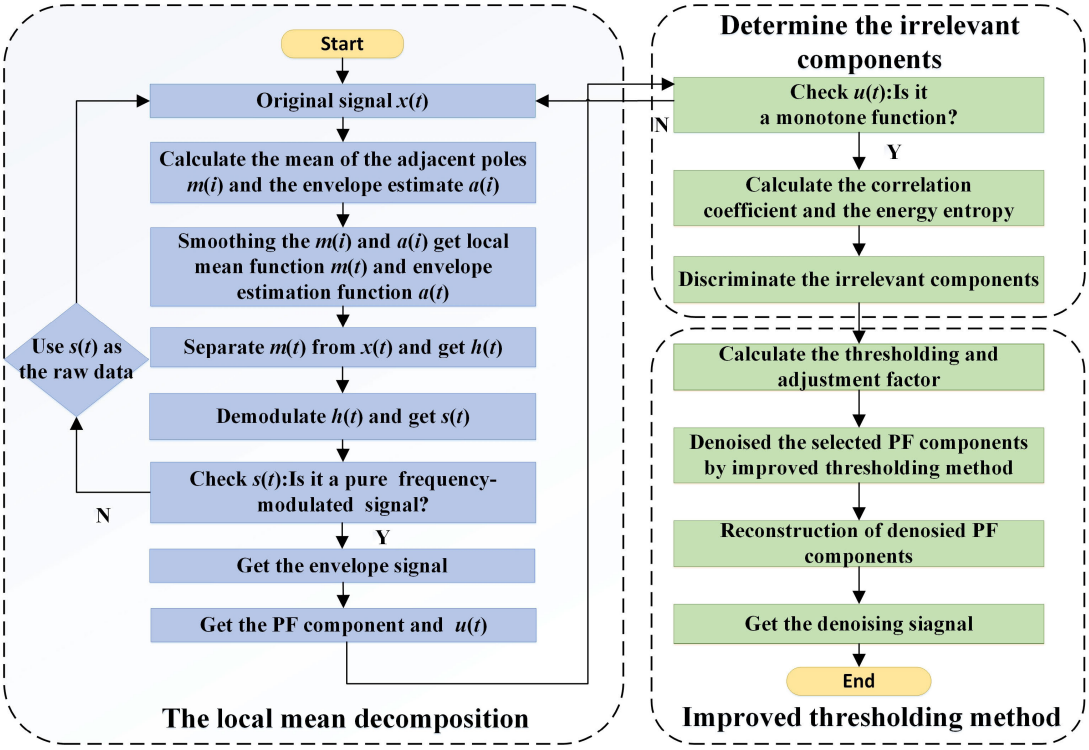

FIGURE 2. Pictorial representation of LMD-ITM.

satisfy $a_{12}(t) = 1$, this proves that $s_{11}(t)$ is a pure frequency modulated. If the formula does not hold, then $s_{11}(t)$ is processed as the initial signal until the signal satisfying the condition can be obtained. Therefore, we can get

$$\begin{cases} h_{11}(t) = x(t) - m_{11}(t) \\ h_{12}(t) = s_{11}(t) - m_{12}(t) \\ \vdots \\ h_{1n}(t) = s_{1(n-1)}(t) - m_{1n}(t), \end{cases} \tag{5}$$

where

$$\begin{cases} \mathrm{s}_{11}(t) = h_{11}(t)/a_{11}(t) \\ \mathrm{s}_{12}(t) = h_{12}(t)/a_{12}(t) \\ \vdots \\ \mathrm{s}_{1n}(t) = h_{1\mathrm{n}}(t)/a_{1\mathrm{n}}(t), \end{cases} \tag{6}$$

where the objective is to achieve

$$\lim_{n\to\infty} a_{1n}(t) = 1. \tag{7}$$

Step 5. Then, the continuous function generated in the iterative cycle is multiplied, and the result is taken as the envelope signal $a_1(t)$, which represents the instantaneous amplitude function.

$$a_1(t) = a_{11}(t)a_{12}(t)\cdots a_{1n}(t) = \prod_{q=1}^{n} a_{1q}(t), \tag{8}$$

Step 6. The new product function component shows below:

$$\mathrm{PF}_1(t) = a_1(t)s_{1n}(t), \tag{9}$$

The decomposed signal contains the high-frequency component of the original signal. Meanwhile, the its instantaneous amplitude is exactly equal to $a_1(t)$ and instantaneous frequency from the $s_{1_n}(t)$, as shown below:

$$f_1(t) = \frac{1}{2\pi}\frac{d[\arccos(s_{1n}(t))]}{dt}. \tag{10}$$

Step 7. $u_1(t)$ is obtained by subtracting the high-frequency component from the original signal. In order to decompose the signal thoroughly, the above process is repeated again with the new signal as the original signal until $u_p \leq 1$, then the operation will stop.

$$\begin{cases} u_1(t) = x(t) - \mathrm{PF}_1(t) \\ u_2(t) = u_1(t) - \mathrm{PF}_2(t) \\ \quad \vdots \\ u_k(t) = u_{k-1}(t) - \mathrm{PF}_k(t). \end{cases} \tag{11}$$

Thus, the $x(t)$ is decomposed into p-product and a monotonic function u_k

$$x(t) = \sum_{p=1}^{k} \mathrm{PF}_p(t) + u_k(t). \tag{12}$$

By decomposing the original signal into a series of components, we can interpret the original signal more accurately for qualitative and quantitative.

III. PRINCIPLE BEHIND LMD-ITM FOR NOISE REDUCTION

Fig. 2 shows the flow of LMD-ITM method. The main process of this algorithm can be divided into three modules.

The first part is the local mean decomposition, which includes an inner loop and an outer loop to achieve signal decomposition. In the second part, the correlation coefficient and energy entropy are used to determine whether the components contain a large amount of noise. The third part is the improved thresholding method, which is based on the traditional thresholding using the denoising method. The improved thresholding method realizes adaptive and effective filtering by calculating the thresholding and adjustment factor. It can extract the effective signals which are difficult to be separated from the high-frequency signals. Finally, the processed components and other components are selected to reconstruct the LiDAR signal.

A. IDENTIFICATION METHODS OF THE CORRELATION COMPONENTS

The aim of the experiment is denoising the observed signal $x(t)$ and getting estimate signal $h(t)$. After using LMD method to dispose of the noise in the signal, we need pick out the components with a lot of noise to filter, retain the appropriate components to recombine them at the same time, the formula is as follows:

$$h(t) = \sum_{p=k_{th}}^{k} PF_p(t) + u_k(t), \tag{13}$$

where $\mathrm{PF}_p(t)$ represents a collection of the decomposed PF. It can calculate the correlation coefficient and energy entropy to determine the index k_{th} for the components of reconstruction, $u_k(t)$ represents the final residual. The estimated signal $h(t)$ can also be written as

$$h(t) = x(t) - \sum_{p=1}^{k} PF_p(t), \tag{14}$$

where p is the number of layers. The degree of similarity between $x(t)$ and $h(t)$ needs to be expressed by calculating a specific correlation coefficient:

$$\rho_p = \frac{\sum_{n=1}^{N} x(t)h_p(t)}{\sqrt{\sum_{n=1}^{N} x^2(t) \sum_{n=1}^{N} (h_p)^2(t)}} \tag{15}$$

in this formula the N represent the total length of the signal. The ρ_P always decreases until to minimum. The k_{th1} is given by

$$k_{th1} = \arg last_{1\le p\le k} \left\{\rho_p \ge B_1\right\} + 1. \tag{16}$$

In general, the value of B_1 belongs to the interval [0.75, 0.85]. The denoising results of different B_1 values in this range are compared by experiment. In this study, B_1 is set to 0.85, the result can obtain the highest SNR_{out} [21].

After the $x(t)$ is decomposed using LMD, the final residual $u(t)$ and the PF components are obtained. The $E_1, E_2, \cdots, E_k$ can calculated by specific formula to express the value of energy contained in each PF component. [22]–[24]. The value of energy in the residual component $u(t)$ is extremely weak. Therefore, the sum the energies of the PF components without the residual energy is equal the total energy of the original signal [25]. The energy entropy H_p is calculated by

$$H_p = -E_P \Big/ \sum_{p=1}^{k} E_p \times (\log_2 (E_P \Big/ \sum_{p=1}^{k} E_p)). \tag{17}$$

The value of k_{th2} is given by

$$k_{th2} = \arg last_{1\le t\le p} \left\{H_p \ge B_2\right\} + 1. \tag{18}$$

Here, the value B_2 belongs to the interval [0.25, 0.35]. The denoising results of different B_2 values in this range are compared by experiment. When the B_2 is set to 0.25, we can get the best denoising effect. Through the above process, the value $k_{th} = min\{k_{th1}, k_{th2}\}$ can be determined. Thus, the components before the k_{th} component are irrelevant.

B. LMD COMBINED WITH THE IMPROVED THRESHOLDING METHOD

In recent years, some studies have shown that combining the threshold technology with the decomposition algorithm can significantly reduce the noise and retain the effective information in the high-frequency components [26]. The thresholding method has the advantages of fast calculation speed and original signal approximation, and thus it has widely used in denoising algorithms.

However, there are still some disadvantages in the traditional thresholding method. The hard thresholding method ensures that the noise is almost completely suppressed, but it easily generates local mutations in the reconstructed signal. The soft thresholding is compressed by a fixed value, but it is very difficult to choose a suitable fixed value.

In this paper, an improved adaptive thresholding method is used to process the irrelevant components, to extract the useful signals effectively [27].

$$\overline{PF_p} = \begin{cases} PF_p - \dfrac{\beta_p \lambda_p^2}{\lambda_p + PF_p} & PF_p \ge \lambda_p \\ 0 & \left|PF_p\right| < \lambda_p \\ PF_p + \dfrac{\beta_p \lambda_p^2}{\lambda_p - PF_p} & PF_p \le -\lambda_p, \end{cases} \tag{19}$$

where $\lambda_p = \sigma_p\sqrt{2\ln N}$ is the universal thresholding, $\sigma_p = median\left(\left|PF_p - median(PF_p)\right|\right)/0.6745$ is the estimated noise level of the PF_P., $median(PF_P)$ represents the median of PF_P.

The adjustment factor β_p can be determined in three steps:

Step 1. Calculate the maximum value of the adjustment factor $\beta_{p,\max} = [\mu_p + max(\left|PF_p\right|)]/\delta_p$, where δ_p represents the standard deviation of the PF component and the μ_p represents the mean.

Step 2. Calculate the peak ratio of the PF component using $S_p = \max\left|PF_p\right|/\sum PF_p$, where S_p can reflect the sparsity of the component, and the amount of useful information and noise in the PF component. When $S_P < T_r$ and $S_{P+1} < T_r$, the number of layers p is considered as the optimal number of local mean decomposition layers q. After analysing a large number of experimental data, it can be concluded that

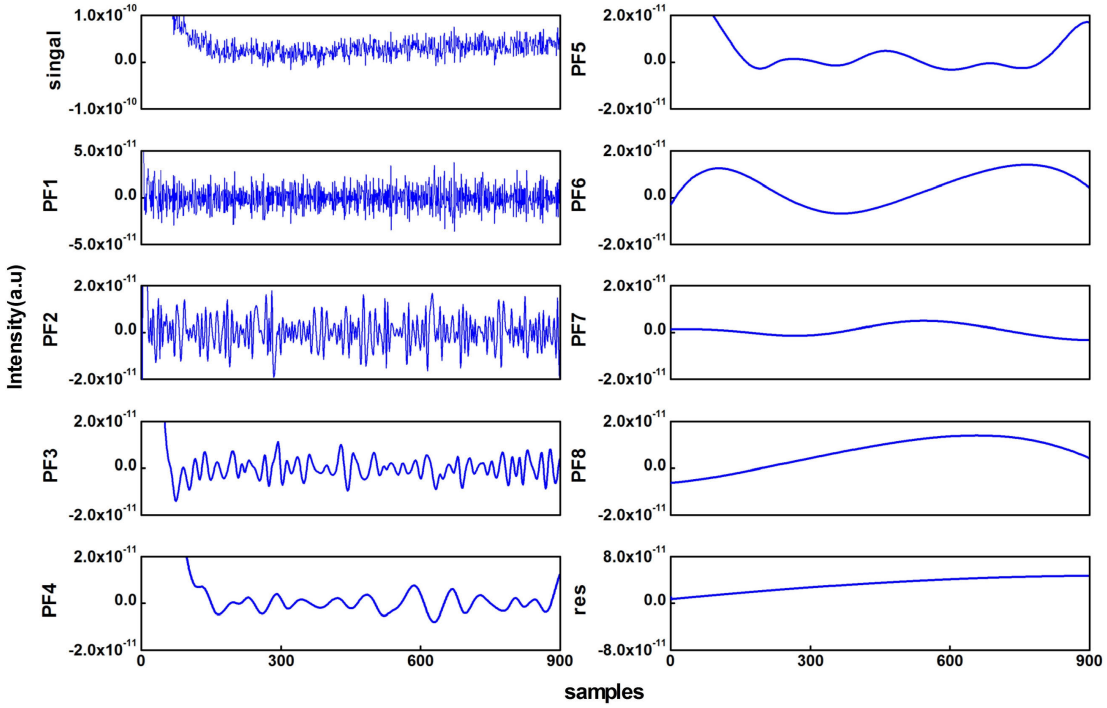

FIGURE 3. The PF components arranged from high-frequency to low-frequency.

when $T_r = 0.06$, we can effectively distinguish whether the PF component contains noise information.

Step 3. Based on the distribution characteristics of the useful information and noise in the PF component of layer p and the peak ratio, the adjustment factors for the threshold values of each layer $\beta_p = \left(1 - \frac{S_p}{S_q + S_{q+1}}\right)\beta_{p,\max}$ can be obtained.

The improved thresholding method overcomes the weakness of soft thresholding fixed shrinkage and solves the hard thresholding discontinuity to compensate for its local oscillation. It effectively reduced the risk of signal distortion.

IV. RESULTS AND DISCUSSION

A. DENOSING PERFORMANCE FOR SIMULATED SIGNAL

The established output *SNR* (denoted by SNR_{out}) and root mean square error (RMSE) are the indexes, which are displayed by specific values. The value of SNR_{out} can well reflect the content of useful information in a signal, the more useful information in the signals, the values of SNR_{out} would be higher. Likewise, a smaller RMSE indicates a greater similarity between the two signals. The SNR_{out} and RMSE values can be calculated as follows:

$$SNR_{\text{out}} = 10\log\left(\frac{\sum_{t=1}^{N}|x(t)|^2}{\sum_{t=1}^{N}|x(t)-x^*(t)|^2}\right), \tag{20}$$

$$RMSE = \sqrt{\frac{1}{N}\sum_{t=1}^{N}(x(t)-x^*(t))^2}, \tag{21}$$

In the above formula, $x(t)$ represents the original signal and $x^*(t)$ represents the denoised signal.

We add 5dB White Gaussian noise and the photon shot noise to the pure LiDAR signal to synthesize a simulated signal. It shows the decomposition of the simulated signal into eight components by LMD method, and the components distributed from the high to low frequencies in Fig. 3. It is well established that LMD method removes the high-frequency components gradually. As shown in the figure, compared with the other components, the first component contained the maximum energy, which included the highest frequency [28]. This implies that several PF components in front contain most of the noise in the LiDAR signal, as these components will be processed further.

Fig. 4 shows the correlation coefficient with different PF components in a curvilinear way and the histogram of the PF energy entropy. According to (16) and (18), the optimum value of k_{th} is set to 3, and PF3 to PF8 is set as the relevant component.

The results of processing noisy simulated signals by two different denoising methods show in Fig. 5. The improved thresholding method could adaptively filter out the noise in the simulated signal according to the PF component, effectively reduce the influence of White Gaussian noise and photon shot noise in the signal and greatly improve the SNR.

It carries out experiments on the simulated signals with different degree of noise interference. Table 1 lists the values of SNR_{out}/RMSE of the two methods after the denoising of the simulated signals when the SNR_{in} values varying from 1 dB to 8 dB. In this table the values of SNR_{out} are before the slash and the values of RMSEs are after the slash. It can

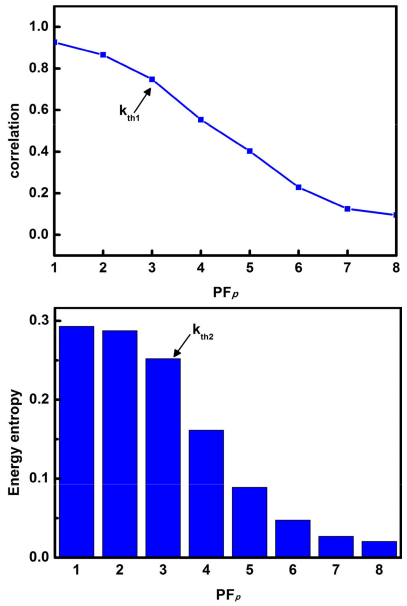

FIGURE 4. Curve of correlation coefficient with PF_p and histogram of PF_p energy entropy.

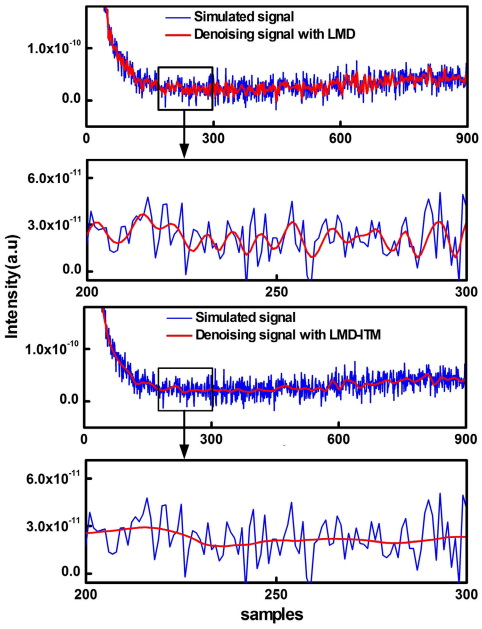

FIGURE 5. The results of processing noisy simulated signal by LMD and LMD-ITM methods.

be seen from this experiment that the proposed method is superior and stable.

B. EXPERIMENTS ON REAL LIDAR SIGNAL

We apply the LMD-ITM method to real data measured using a ground-based LiDAR. The Nanjing University of Information Science & Technology (118.7 °N, 32.2 °E) recorded the systematic observation of the aerosol extinction coefficient. This experiment uses the Rayleigh-Raman-Mie LiDAR developed by the Anhui Institute of Optics and Fine Mechanics, Chinese academy of sciences [29]. The LiDAR system consists of a diode-pumped Nd:YAG laser with a pulse output wavelength of 532 nm, the repetition frequency of 20 Hz, and the pulse energy of 200 mJ. The receiving element consists of the Cassegrain telescope with a diameter of 400 mm and a field of view of 2 mrad. A photomultiplier receives the laser radar echo signal with a range resolution of approximately 30 m. The working principle of LiDAR system is described as follows: Firstly, the laser pulse is generated by the synchronous trigger of the laser module, and then the light is fed into the fiber through a coupler. The telescope accomplishes the transmitting of the laser pulse and receiving of the echo signals. Finally, the photoelectric conversion is carried out by a photoelectric detector, and the data is collected and transmitted to the upper computer. After getting the echo signal, the signal should be pre-processed, including geometric overlap factor correction and range square correction, etc.

TABLE 1. Denoising performance of the LMD and LMD-ITM.

SNR_{in}	1dB	2dB	3dB	4dB
LMD	5.79/2.83	7.23/2.40	8.21/2.14	9.63/1.80
LMD-ITM	11.27/1.51	13.63/1.14	14.31/1.06	15.91/0.87
SNR_{in}	5dB	6dB	7dB	8dB
LMD	10.69/1.61	11.95/1.39	13.43/1.17	14.31/1.06
LMD-ITM	16.32/1.39	17.47/0.93	19.29/0.67	20.45/0.58

In the actual observation, the echo signal received by the telescope is limited. The reason behind this phenomenon is that the axial directions of the LiDAR transmission and receiving systems are different. Therefore, we use the geometric overlap factor (GOF) [30] to correct the received signal. Fig. 6 shows the application of WT, LMD, CEEMDAN, EMD-STRP, VMD-WOA, and LMD-ITM in removing noise from the GOF-corrected signal. The signal at 1.2–2 km is amplified locally, which can depict the denoising effect clearly. In the figure, LMD only removes the high-frequency signal by modal decomposition without achieving true denoising, with the signal remaining significantly noisy. Due to the endpoint effect, the denoising results by EMD-STRP method deviated from the original signal at 1.2 km. In the short-range, the signal processed by the VOM-WOA method is too smooth, which causes the denoising signal deviated completely from the original signal. In contrast, the result of LMD-ITM fit the original signal almost without any deviation. This experiment proves that LMD-ITM method can effectively avoid the phenomenon of short-range offset.

In addition to the influence of the noise on the LiDAR signal, distance is also an important factor. The intensity of the LiDAR signal changed according to the distance, when the distance of the signal is longer, the attenuation of SNR is more serious. The range square corrected (RSC) signal is calculated by multiplying the signal by the square of the

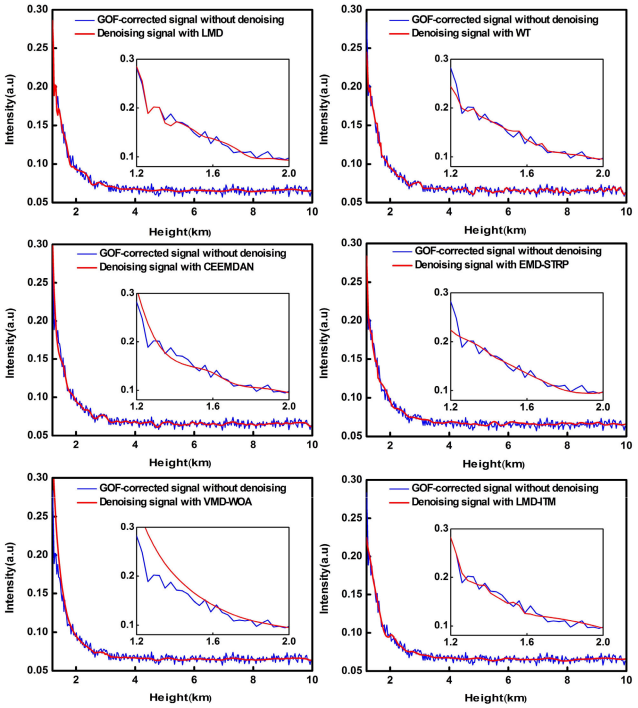

FIGURE 6. Comparison of denoising results of the GOF-corrected signal from the LMD-ITM and other methods.

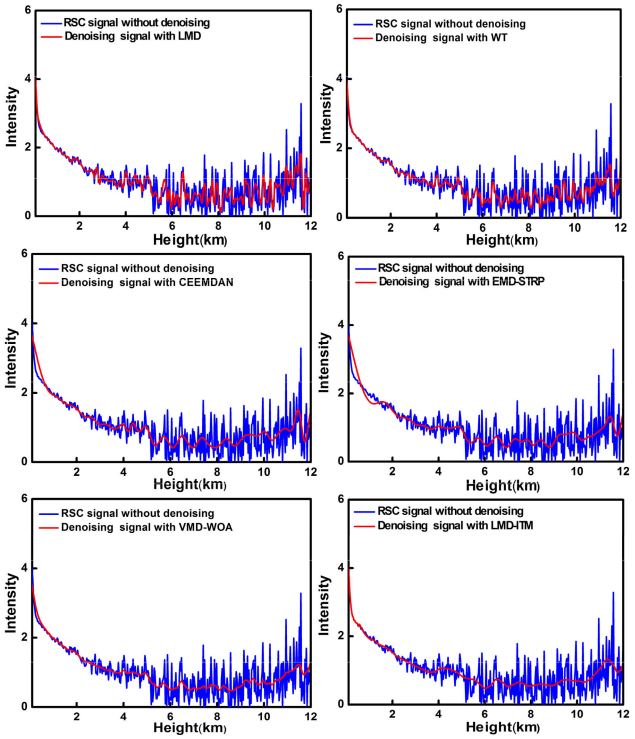

FIGURE 7. Comparison of the six methods for the RSC signal.

distance, and this processing can reduce the influence of the distance on the signal. However, it not only enhances the echo signal but also enhances the noise in the signal. With the increase of distance, the whole signal changes dramatically, and the effective signal strength is gradually reduced and submerged by noise. LMD can decompose the signal into a series of PF components, which are arranged from high-frequency to low-frequency. According to the characteristics of the PF component, the amplitude of the high-frequency components decays rapidly with the increase of the decomposition level, the noise can be filtered out more efficiently, and the valid signal can be extracted from the RSC signal.

Fig. 7 shows the RSC signal after denoising, corresponding to the six kinds of denoising methods. Due to the uncertainty of the thresholding value of WT, the denoised results of WT are not ideal, where the high-frequency signals are not completely filtered. The phenomenon of short-range offset exists in CEEMDAN, EMD-STRP, and VMD-WOA methods in the 1–2 km short-range signal. The figure shows that the echo signal has improved smoothness after denoising using LMD-ITM method, and precisely retains the changing trend of the signal. In addition, the updated signal reduces the interference of noise, as the improved thresholding method is adopted in the optimization process. By comparing with other methods, LMD-ITM method can suppress the sharp change of the long-range signal after 8 km and demonstrate good denoising performance.

$\Delta SNR = [(SNR_L - SNR_W)/SNR_W] \times 100\%$ are calculated as a performance index, where SNR_L and SNR_W represent the *SNR*s of the proposed and traditional methods [31]. The index shows that the improvement of SNR varies with different methods. Then the *SNR*s of LMD-ITM and EMD-STRP are substituted into the formula as a new method and traditional method respectively.

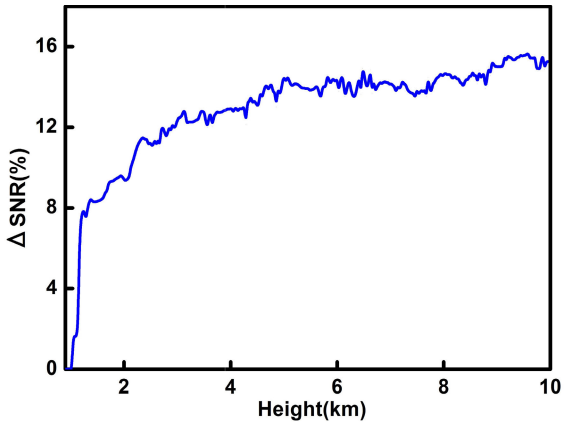

FIGURE 8. The percentage of incremental SNR by LMD-ITM method and EMD-STRP method.

Fig. 8 shows the ΔSNR results, which indicate that ΔSNR increased with the distance. When the distance increases from 1 km to 3 km, the ΔSNR increases sharply from 8% to 12%. Then, as the distance increases from 3 km to 10 km, the ΔSNR increases from 12% to 15%. The results show that the LMD-ITM method had a significant effect on the signal denoising at long-range. Although the ΔSNR will not

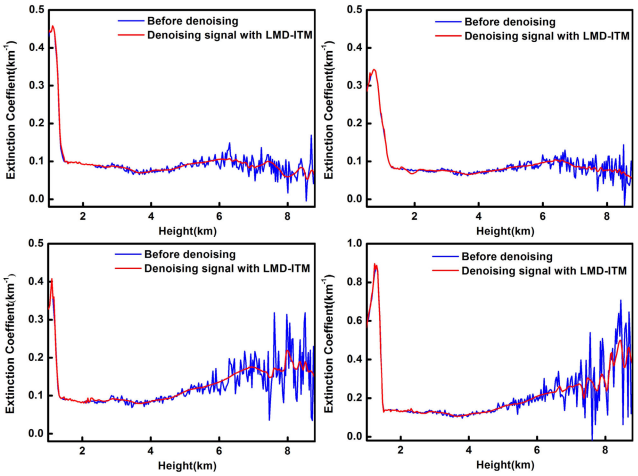

FIGURE 9. The aerosol extinction coefficient profiles under different weather conditions.

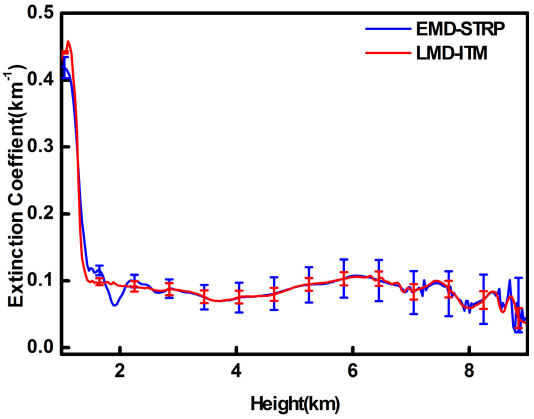

FIGURE 10. The RMSE of the EC profiles retrieved by two kinds of denoising signals.

vary dramatically with increasing distance, it maintains a high value.

C. RETRIEVAL OF THE ATMOSPHERIC EXTINCTION COEFFICIENT PROFILES

In further processing, the aerosol extinction coefficient (EC) can be retrieved based on the denoising signal by the Fernald method [32]. Fig. 9 compares the results of EC profiles under different weather conditions. The blue line and the red line respectively represent the EC profiles, which are retrieved by the before and after denoising signals. The LiDAR data for the experiment were detected on 18, 19, 24, and 25 May 2017. It can be seen from the figure that the EC profiles are retrieved by the denoising signals with LMD-ITM has better smoothness. As the distance increases, the signal strength gradually decreases and becomes noisier. Although the original EC profiles after 6 km gradually became strongly fluctuating, the useful signals still can be extracted from the denoising signal. This highly efficient denoising method can generate an accurate EC profile, thus increasing the availability of data. This experiment shows that the method used in this paper can adapt to different weather conditions, and it has a strong universality.

Fig. 10 illustrates the EC profiles and the RMSE obtained by two kinds of denoising signals. The red and blue curves in the figure represent the EC profiles retrieved by the denoising signals with EMD-STRP and LMD-ITM. The vertical lines represent the RMSE value of this position. The shorter the length of the vertical line, the smaller the RMSE values, which means the lower the error of the result. The two methods have significantly different RMSE, and the LMD-ITM method offers a great advantage with respect to the extinction coefficient inversion both at short and long distances. Thus, the results show that our proposed method had good stability. When distances less than 2 km, a certain deviation of EMD-STRP method can lead to poor denoising effect. Nevertheless, the LMD-ITM method effectively optimizes the problem of short-range offset. With the increase of distance, the RMSE of the EC profile retrieved by EMD-STRP method also increases. However, the RMSE of the EC profile retrieved by the LMD-ITM method is still low, thus indicating that the LMD-ITM method validly restrains the noise in the long-range signal after 8 km.

V. CONCLUSION

A new denoising method is applied to the LiDAR signal, which is named LMD-ITM. The method decomposed the LiDAR signal into different frequency components through LMD. The energy entropy and the correlation coefficient are calculated to select the components related to the pure signal. Subsequently, an adaptive thresholding method is designed to filter the noise and retain useful signals as much as possible. The first experiment uses LMD and LMD-ITM to process the simulated LiDAR signal which contaminates with White Gaussian noise and the photon shot noise. The results show that the improved thresholding method is feasible and effective. In the second experiment, to analyze the denoising effect more intuitively, WT, LMD, CEEMDAN, EMD-STRP, VMD-WOA, and LMD-ITM are used to real LiDAR signal. These tests show that LMD-ITM method reduced the uncertainty in the denoising signal better than the other methods. Furthermore, the results indicate that LMD-ITM method not only eliminates the proximal biases, but also achieves the superior denoising effect in the long-range. As compared with the traditional denoising methods, the proposed LMD-ITM method increases the SNR by about 15%. Finally, the experiment performed that profiles of the aerosol extinction coefficient retrieved from the different denoised signals can prove the generality of LMD-ITM. This method reduces the error in the LiDAR retrieval and improves the performance of LiDAR.

ACKNOWLEDGMENT

The authors would like to thank Lingbing Bu from the School of Atmospheric Physics, Nanjing University of Information Science and Technology, for providing data support and constructive suggestions.

REFERENCES

[1] S. Chudzyński, A. Czyżewski, K. Ernst, G. Karasiński, K. Kolacz, A. Pietruczuk, W. Skubiszak, T. Stacewicz, K. Stelmaszczyk, and A. Szymański, "Multiwavelength lidar for measurements of atmospheric aerosol," *Opt. Laser Eng.*, vol. 37, nos. 2–3, pp. 91–99, 2002.

[2] H. Xia, M. Shangguan, C. Wang, G. Shentu, J. Qiu, Q. Zhang, X. Dou, and J. Pan, "Micro-pulse upconversion Doppler lidar for wind and visibility detection in the atmospheric boundary layer," *Opt. Lett.*, vol. 41, no. 22, p. 5218, 2016.

[3] S. Wu, Z. Liu, and B. Liu, "Enhancement of lidar backscatters signal-to-noise ratio using empirical mode decomposition method," *Opt. Commun.*, vol. 267, no. 1, pp. 137–144, Nov. 2006.

[4] Q. Hao, J. Cao, Y. Hu, Y. Yang, K. Li, and T. Li, "Differential optical-path approach to improve signal-to-noise ratio of pulsed-laser range finding," *Opt. Express*, vol. 22, no. 1, p. 563, 2014.

[5] H.-T. Fang and D.-S. Huang, "Noise reduction in Lidar signal based on discrete wavelet transform," *Opt. Commun.*, vol. 233, nos. 1–3, pp. 67–76, Mar. 2004.

[6] M. Sarvani, K. Raghunath, and S. V. B. Rao, "Lidar signal denoising methods- application to NARL Rayleigh lidar," *J. Opt.*, vol. 44, no. 2, pp. 164–171, Jun. 2015.

[7] F. Rocadenbosch, C. Soriano, A. Comerón, and J.-M. Baldasano, "Lidar inversion of atmospheric backscatter and extinction-to-backscatter ratios by use of a Kalman filter," *Appl. Opt.*, vol. 38, no. 15, p. 3175, 1999.

[8] Z. Zhou, D. Hua, Y. Wang, Q. Yan, S. Li, Y. Li, and H. Wang, "Improvement of the signal to noise ratio of Lidar echo signal based on wavelet de-noising technique," *Opt. Lasers Eng.*, vol. 51, no. 8, pp. 961–966, Aug. 2013.

[9] F. Xu and Y. Wang, "Signal enhancement of a novel multi-address coding lidar backscatters based on a combined technique of demodulation and wavelet de-noising," *Opt. Lasers Eng.*, vol. 74, pp. 122–129, Nov. 2015.

[10] N. E. Huang, Z. Shen, S. R. Long, M. C. Wu, H. H. Shih, Q. Zheng, N.-C. Yen, C. C. Tung, and H. H. Liu, "The empirical mode decomposition and the Hilbert spectrum for nonlinear and non-stationary time series analysis," *Proc. Roy. Soc. London. Ser. A, Math., Phys. Eng. Sci.*, vol. 454, no. 1971, pp. 903–995, Mar. 1998.

[11] M. A. Colominas, G. Schlotthauer, and M. E. Torres, "Improved complete ensemble EMD: A suitable tool for biomedical signal processing," *Biomed. Signal Process. Control*, vol. 14, pp. 19–29, Nov. 2014.

[12] H. Li, J. Chang, F. Xu, Z. Liu, Z. Yang, L. Zhang, S. Zhang, R. Mao, X. Dou, and B. Liu, "Efficient lidar signal denoising algorithm using variational mode decomposition combined with a whale optimization algorithm," *Remote Sens.*, vol. 11, no. 2, p. 126, Jan. 2019.

[13] J. S. Smith, "The local mean decomposition and its application to EEG perception data," *J. Roy. Soc. Interface*, vol. 2, no. 5, pp. 443–454, Dec. 2005.

[14] Z. Yan, B. Hou, J. Zhang, C. Shen, Y. Shi, J. Tang, H. Cao, and J. Liu, "MEMS accelerometer calibration denoising method for Hopkinson bar system based on LMD-SE-TFPF," *IEEE Access*, vol. 7, pp. 113901–113915, 2019.

[15] Y. Cheng and D. Zou, "Complementary ensemble local means decomposition method and its application to rolling element bearings fault diagnosis," *Proc. Inst. Mech. Eng., Part O, J. Risk Rel.*, vol. 233, no. 5, pp. 868–880, Oct. 2019.

[16] M. Le Van Quyen, J. Foucher, J.-P. Lachaux, E. Rodriguez, A. Lutz, J. Martinerie, and F. J. Varela, "Comparison of Hilbert transform and wavelet methods for the analysis of neuronal synchrony," *J. Neurosci. Methods*, vol. 111, no. 2, pp. 83–98, Sep. 2001.

[17] N. E. Huang and Z. Wu, "A review on Hilbert-Huang transform: Method and its applications to geophysical studies," *Rev. Geophys.*, vol. 46, no. 2, p. G2006, 2008.

[18] Y. Wang, Z. He, and Y. Zi, "A comparative study on the local mean decomposition and empirical mode decomposition and their applications to rotating machinery health diagnosis," *Trans. ASME*, p. 132, 2010.

[19] Z. Wang, J. Wang, W. Cai, J. Zhou, W. Du, J. Wang, G. He, and H. He, "Application of an improved ensemble local mean decomposition method for gearbox composite fault diagnosis," *Complexity*, vol. 2019, pp. 1–17, May 2019.

[20] W. Y. Liu, W. H. Zhang, J. G. Han, and G. F. Wang, "A new wind turbine fault diagnosis method based on the local mean decomposition," *Renew. Energy*, vol. 48, pp. 411–415, Dec. 2012.

[21] Y. Duan and C. Song, "Relevant modes selection method based on spearman correlation coefficient for laser signal denoising using empirical mode decomposition," *Opt. Rev.*, vol. 23, no. 6, pp. 936–949, Dec. 2016.

[22] Z. Wang, J. Wang, and W. Du, "Research on fault diagnosis of gearbox with improved variational mode decomposition," *Sensors*, vol. 18, no. 10, p. 3510, Oct. 2018.

[23] L. Zhao, S. Wei, C. Zhang, Y. Zhang, X. Jiang, F. Liu, and C. Liu, "Determination of sample entropy and fuzzy measure entropy parameters for distinguishing congestive heart failure from normal sinus rhythm subjects," *Entropy*, vol. 17, no. 12, pp. 6270–6288, Sep. 2015.

[24] Y. Wu, P. Shang, and Y. Li, "Modified generalized multiscale sample entropy and surrogate data analysis for financial time series," *Nonlinear Dyn.*, vol. 92, no. 3, pp. 1335–1350, May 2018.

[25] Z. Wang, J. Zhou, J. Wang, W. Du, J. Wang, X. Han, and G. He, "A novel fault diagnosis method of gearbox based on maximum kurtosis spectral entropy deconvolution," *IEEE Access*, vol. 7, pp. 29520–29532, 2019.

[26] G. Yang, Y. Liu, Y. Wang, and Z. Zhu, "EMD interval thresholding denoising based on similarity measure to select relevant modes," *Signal Process.*, vol. 109, pp. 95–109, Apr. 2015.

[27] M. Srivastava, C. L. Anderson, and J. H. Freed, "A new wavelet denoising method for selecting decomposition levels and noise thresholds," *IEEE Access*, vol. 4, pp. 3862–3877, 2016.

[28] H. Liu and M. Han, "A fault diagnosis method based on local mean decomposition and multi-scale entropy for roller bearings," *Mech. Mach. Theory*, vol. 75, pp. 67–78, May 2014.

[29] J. Chang, L. Zhu, H. Li, F. Xu, B. Liu, and Z. Yang, "Noise reduction in Lidar signal using correlation-based EMD combined with soft thresholding and roughness penalty," *Opt. Commun.*, vol. 407, pp. 290–295, Jan. 2018.

[30] I. Berezhnyy, "A combined diffraction and geometrical optics approach for lidar overlap function computation," *Opt. Lasers Eng.*, vol. 47, nos. 7–8, pp. 855–859, Jul. 2009.

[31] Y. Cheng, J. Cao, Q. Hao, Y. Xiao, F. Zhang, W. Xia, K. Zhang, and H. Yu, "A novel de-noising method for improving the performance of full-waveform LiDAR using differential optical path," *Remote Sens.*, vol. 9, no. 11, p. 1109, Oct. 2017.

[32] H. Li, J. Chang, F. Xu, B. Liu, Z. Liu, L. Zhu, and Z. Yang, "An RBF neural network approach for retrieving atmospheric extinction coefficients based on lidar measurements," *Appl. Phys. B, Lasers Opt.*, vol. 124, no. 9, p. 184, Sep. 2018.

LUYAO ZHANG was born in Jiangsu, China. She is currently pursuing the master's degree with the Jiangsu Key Laboratory of Meteorological Observation and Information Processing, Nanjing University of Information Science and Technology, Nanjing, Jiangsu. Her current research interests include LiDAR measurements and signal processing.

JIANHUA CHANG was born in Jiangsu, China. He received the Ph.D. degree from the Department of Electronic Engineering, Southeast University. He was a Postdoctoral Fellow with the Anhui Institute of Optical Mechanics, Chinese Academy of Sciences, and McMaster University, Canada. He is currently the Deputy Dean of the School of Electronics and Information Engineering, Nanjing University of Information Technology. His current research interests include photonics and optical devices, all-solid-state lasers, LiDAR, and photoelectric sensing. He is a member of the Optoelectronic Technology Committee of the China Optical Society and a Senior Member of the China Electronics Society.

HONGXU LI was born in Henan, China. He is currently pursuing the Ph.D. degree with the Jiangsu Key Laboratory of Meteorological Observation and Information Processing, Nanjing University of Information Science and Technology, Nanjing, Jiangsu. His current research interests include LiDAR measurements and aerosol detection.

ZHEN XING LIU was born in Jiangsu, China. He is currently pursuing the Ph.D. degree with the Jiangsu Key Laboratory of Meteorological Observation and Information Processing, Nanjing University of Information Science and Technology, Nanjing, Jiangsu. He is currently working in electronics and information engineering with the Taizhou Polytechnic College. His current research interests include LiDAR measurements and signal processing.

SHUYI ZHANG was born in Jiangsu, China. She is currently pursuing the master's degree with the Jiangsu Key Laboratory of Meteorological Observation and Information Processing, Nanjing University of Information Science and Technology, Nanjing, Jiangsu. Her current research interests include LiDAR and 3-D point cloud processing.

RENGXIANG MAO was born in Jiangsu, China. He is currently pursuing the master's degree with the Jiangsu Key Laboratory of Meteorological Observation and Information Processing, Nanjing University of Information Science and Technology, Nanjing, Jiangsu. His current research interests include LiDAR measurements and 3-D point cloud processing.